



HAL
open science

Direct etching at the nanoscale through nanoparticle-directed capillary condensation

M. Garín, R. Khoury, I. Martín, Erik Johnson

► **To cite this version:**

M. Garín, R. Khoury, I. Martín, Erik Johnson. Direct etching at the nanoscale through nanoparticle-directed capillary condensation. *Nanoscale*, 2020, 12 (16), pp.9240-9245. 10.1039/C9NR10217E . hal-03001169

HAL Id: hal-03001169

<https://hal.science/hal-03001169v1>

Submitted on 23 Nov 2020

HAL is a multi-disciplinary open access archive for the deposit and dissemination of scientific research documents, whether they are published or not. The documents may come from teaching and research institutions in France or abroad, or from public or private research centers.

L'archive ouverte pluridisciplinaire **HAL**, est destinée au dépôt et à la diffusion de documents scientifiques de niveau recherche, publiés ou non, émanant des établissements d'enseignement et de recherche français ou étrangers, des laboratoires publics ou privés.

Direct etching at the nanoscale through nanoparticle-directed capillary condensation.

M. Garín,^{1,2*} R. Khoury,³ I. Martín,¹ E.V. Johnson³

¹ Grup de recerca en Micro i Nanotecnologies, Departament d'Enginyeria Electrònica, Universitat Politècnica de Catalunya, c/ Jordi Girona Pascual 1-3, Barcelona 08034, Spain

² GR-MECAMAT, Department of Engineering, Universitat de Vic – Universitat Central de Catalunya, c/ de la Laura 13, 08500 Vic, Spain

³ Laboratoire de Physique des Interfaces et des Couches Minces (LPICM), CNRS, Ecole Polytechnique, Institut Polytechnique de Paris, 91128 Palaiseau, France.

* Corresponding author: moises.garin@uvic.cat

We report on a method to locally deliver at the nanoscale a chemical etchant in vapor phase by capillary condensation in a meniscus at a nanoparticle/substrate interface. The process is simple, scalable and does not require functionalization of the nanoparticles. Furthermore, it does not rely on any specific chemical properties of the materials other than the solution being aqueous and the wettability properties of the surfaces involved, which should enable its application to other materials and chemicals combinations. In particular, in this work we demonstrate the proposed process by periodically patterning a SiO₂ layer using a self-assembled monolayer of polystyrene particles exposed to HF vapor. The patterned SiO₂ layer is then used as a mask to etch a pattern of inverted nanopyramids in Si. The silicon nanopatterning has been demonstrated for particles sizes from 800 nm down to 100 nm, achieving pyramids with a size down to 50 nm for 100 nm nanoparticles.

1 Introduction

The ability to pattern and structure materials at the nanoscale has enabled a rapid expansion of nanotechnology during the past decades. In particular, not only is it essential for the microelectronic industry¹ but also for the development of metamaterials,^{2,3} metasurfaces,⁴ plasmonics⁵ and nanophotonics,⁶ just to name a few examples. Although some applications can benefit from random nanostructuring techniques,⁷ sophisticated and expensive nanolithography technologies are typically required, such as extreme UV lithography,⁸ electron beam lithography,⁹ ion beam lithography,¹⁰ nanoimprint lithography¹¹ or scanning probe lithography.^{12,13} In addition to these, alternative low-cost self-assembly nanopatterning methods have been proposed such as block copolymers¹⁴ and, most relevant to this work, colloidal lithography.^{15–20}

Colloidal lithography, sometimes called nanosphere lithography, relies on colloidal solutions of, most typically, polystyrene or silica micro-/nano-spheres with a very low size dispersion. These nanospheres can then be self-assembled over large areas, either flat or irregular,¹⁵ adopting a close-packed arrangement that will act either as shadow mask for deposition¹⁸ or as etching mask.¹⁹ Due to its characteristics, colloidal lithography is usually combined with dry etching techniques. Reversing the pattern, *i.e.* etching under the spheres, requires extra steps usually including sphere shrinking and depositing a sacrificial layer. Recently, it has been proposed that functionalized microspheres can be used to locally promote etching around the particles.²⁰ In this way, silicon pyramids were etched into silicon at the locations defined by single particles. However, this method

seems to work at a particle size scale and, therefore, it does not seem feasible to apply it on a close-packed self-assembled layer as it will most probably lead to the etching of the whole surface.

In this paper we demonstrate the use of nanospheres to locally deliver etchant in vapor phase by capillary condensation at the bottom of the spheres. By precisely controlling the partial pressures of water and etchant in vapor phase, the etching can be promoted in a region much smaller than the actual size of the particle and, as a result, the technique can be used with close-packed arrangements of nanospheres. As a demonstration, we have used the process to pattern a layer of SiO₂ with an array of nanoholes by using hydrogen fluoride (HF) vapor. This layer is then used as a mask to create different arrays of nanopyramids in silicon with pyramid sizes as small as 50nm in size and 100nm in pitch.

2 Results and discussion

The samples were prepared as follows. First, a 30nm dry oxide was thermally grown on a standard polished silicon <100> oriented wafer, which was then cleaved into small samples of 1 cm². A close-packed monolayer of polystyrene nanoparticles (PS-NPs) was then deposited over the surface of the samples using the floating-transfer technique.²¹ Four different nominal particle sizes were used namely 800 nm, 600 nm, 400 nm and 100 nm, which were obtained as a 5% aqueous suspension (Microparticles GmbH) and that were further diluted in an equal volume of ethanol as a spreading agent. The monolayers were created at the water/air interface inside a petri dish, transferred onto the surface of the substrates, and allowed to dry in ambient air conditions. This process is shown schematically in Figure 1a—c, while figure 1d shows a photograph of two typical monolayer samples.

Once dry, the samples were etched in HF vapor ambient, as follows. The etching was performed in a home-made set-up (see Fig. 1e) at 25 °C and under atmospheric pressure conditions. Due to the HF toxicity, the set-up was placed in a fume hood to avoid accidental exposure to both HF spills and HF vapors. The reaction chamber has a volume of 1L, and its ambient is controlled by mixing dry N₂ and N₂ saturated with HF + H₂O vapors at specific flow rates. Saturation is achieved by bubbling N₂ through a 5% HF aqueous solution at room temperature, which should reach a partial equilibrium pressure of 22.6 mmHg for H₂O and 0.11 mmHg for HF,²² representing a HF concentration of 147 ppm in the saturated flow. The sample is placed in the reaction chamber and is subjected to four cycles following the following three-step pattern: a) 10 min with 140 sccm of saturated N₂, b) 10 min with 140 sccm of saturated N₂ + 200 sccm of dry N₂, and c) 10 min with 200 sccm dry N₂. During this process, a HF-rich meniscus form between the particles and the sample surface (Fig. 1f), which locally etches the SiO₂ layer (Fig. 1g). After the four cycles the PS monolayer is removed from the sample surface and inverted pyramids are created by immersing the sample 5 min. in 25% tetramethylammonium hydroxide (TMAH) solution (25%) at 85 °C (Fig. 1h). Just before the TMAH etch, we performed a short dip (10") in HF (5%) to remove the native oxide from the opened pattern. Figure 2 shows scanning electron microscope (SEM) images, top view, of both the initial close-packed monolayer of spheres and the arrays of inverted pyramids obtained after the process. Further details and comments on the inverted pyramid formation is included in the supplementary information.

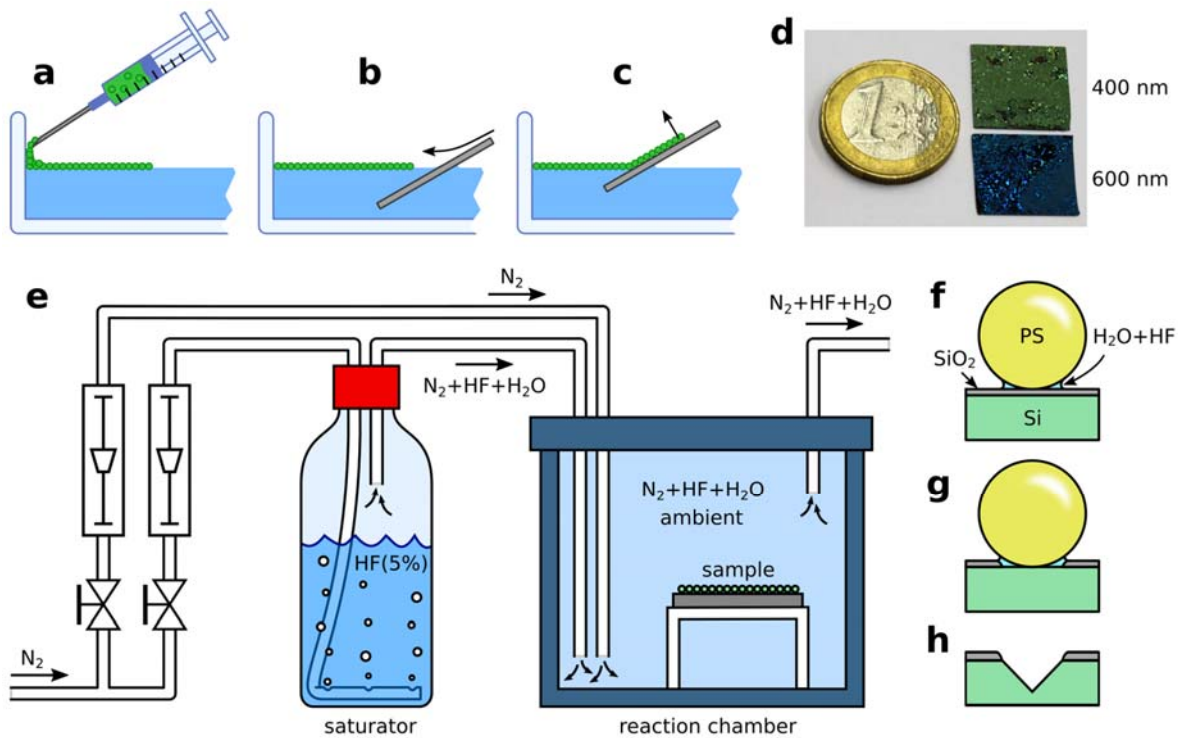


Figure 1. (a–c) Schematic of close-packed monolayer sample preparation. (d) Photography of typical samples after monolayer preparation. (e) Schematic of the HF-vapor etching set-up. (f–g) Schematic of the nanotexturization process: formation of a HF-rich meniscus (f), local etching of the SiO_2 (g) and formation of pyramids in standard TMAH solution (h).

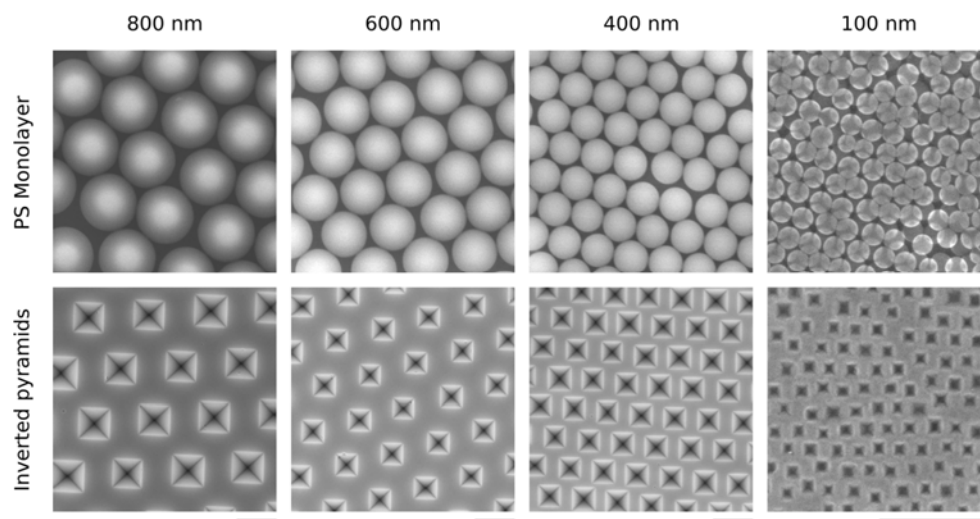


Figure 2. Scanning electron microscopy images of different PS sphere monolayers prepared (top row) and resulting pyramid arrays after full process (bottom row). From left to right, the PS microspheres used had a diameter of 800 nm, 600 nm, 400 nm and 100 nm. All scalebars represent 500nm.

The experimental routine was determined after several tests based on the dynamics of capillary condensation, which is slow and can take several minutes to reach the equilibrium condition.²³ Additionally, the process is further slowed down by the dynamics of the chamber ambient stabilization after changes in the flow rates. During the first step of each cycle the samples are exposed to a 100% relative humidity (RH) ambient with 147 ppm of HF, which induces a quick formation of water + HF menisci at the bottom of the particles, promoting the SiO₂ etching there. If this ambient is maintained for a long time, the menisci slowly grow in excess inducing the complete wetting and etching of the surface. Furthermore, even in the absence of nanospheres, HF vapors eventually condensate and etch the SiO₂ layer everywhere,²⁴ as has been studied in the same setup. To avoid this, the ambient is diluted with dry N₂ in the second step, reducing the RH to 40% and HF concentration to 60 ppm, approximately. The HF-rich water menisci are maintained in this stage thanks to the hysteresis of the meniscus formation/destruction process.²⁵ The last step, only with dry N₂ ambient, dries the structure before the next cycle, to avoid accumulation of condensation over several cycles. Although not strictly necessary for the process, we have noticed that the drying step offers a better control of the menisci formation, therefore improving the definition of the etching and slightly reducing the final pyramid sizes.

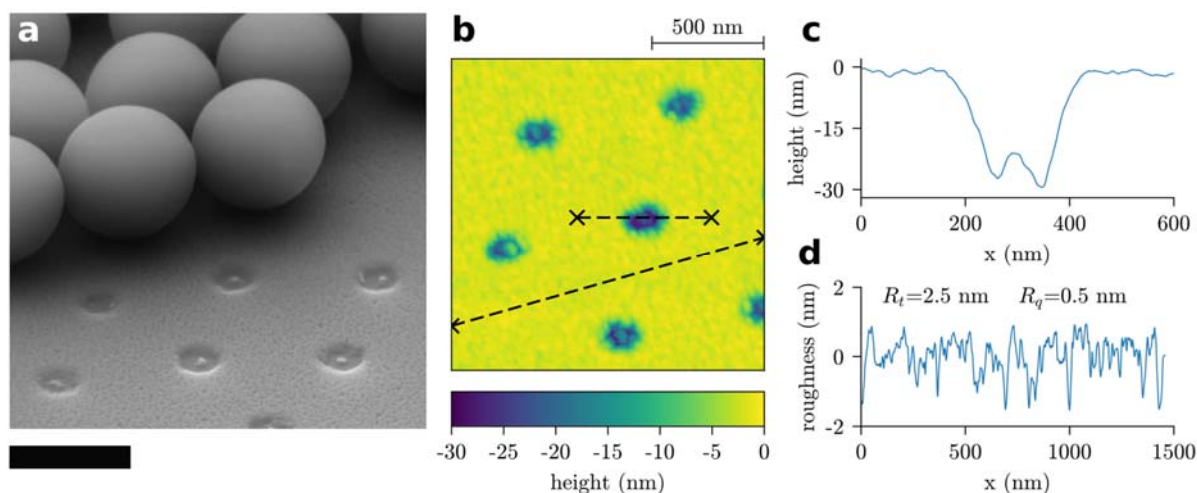


Figure 3. SEM image (a) and AFM image (b) of the SiO₂ surface right after HF vapor etching for a sample with 600 nm spheres. Panels (c) and (d) shows the surface profiles following paths indicated in the AFM image.

Figure 3a shows an SEM image of the surface of one sample with 600 nm nanospheres right after the vapor etching (after four cycles of the process), where a few spheres were removed in order to reveal the SiO₂ surface. In the SEM image, one notes that at most of the sphere locations, the 30nm SiO₂ layer has been completely removed and the Si surface is clearly visible through the resulting opening. A small SiO₂ spot, around 35nm in diameter, is still usually present in the center of the etched areas, which we believe is due to a masking effect at the particle/SiO₂ contact point.

We further investigated the surface of the etched samples through atomic force microscopy (AFM). Figure 3b shows an AFM image of a $1.4\mu\text{m}\times 1.4\mu\text{m}$ region without nanospheres. The profile through one of the openings is shown in Fig. 3c, revealing a maximum etch depth of 30nm, also suggesting a complete removal of the oxide layer after four cycles of vapor etching. Notice that the AFM image at the openings is limited by the shape of the tip, which does not allow one to clearly see the bottom of the openings. Furthermore, the height of the small SiO_2 spot is significantly lower than the initial SiO_2 layer height. This small spot is not significant for the subsequent process, as any remaining oxide in the etched openings will be removed during the 10 seconds HF dip prior to the TMAH etching, which we estimated to remove around 8 nm of SiO_2 . This etching rate estimation was consistently obtained both through ellipsometry measurements and through repeated dipping until completely removing the SiO_2 on reference samples.

Another interesting feature that both the SEM and AFM images reveal is the roughening of the remaining SiO_2 layer. This roughening can be attributed to the direct etching of the SiO_2 by the HF vapors. A roughness analysis of the AFM images, see Fig. 3d, shows a root mean squared (RMS) roughness of $R_q=0.5\text{nm}$ and a total roughness $R_t=2.5\text{ nm}$. This roughening occurred just at the top surface and did not induce any appreciable reduction of the total layer thickness, as the 30 nm height can still be observed at the openings (Fig. 3c). Furthermore, no thickness difference could be measured through ellipsometry, before and after the HF vapor etching, using a reference sample with 100 nm SiO_2 .

The difference in the etching rates between the capillary condensates and the rest of the surface is remarkable, particularly considering that SiO_2 is a hydrophilic surface that is easily etched by HF vapors. This etching selectivity induced by the capillary condensation strongly suggests that this technique might be applicable to a broad range of substrates and chemical agents. Finally, it is worth pointing out that the progressive roughening of the SiO_2 surface is a critical aspect. It enhances condensation and, therefore, increases the etching rate of SiO_2 , which might eventually become a limiting factor to the selectivity of the process. This effect distinctly manifests when exposing oxidized samples just to N_2 ambient with $\text{RH}>90\%$ and HF vapors (step 1 conditions, without any drying step) but for an extended time. Under these conditions the sample eventually develops a thick liquid layer visible to the naked eye that eventually etches the entire SiO_2 layer. In contrast, no such liquid layer is observable after exposing the sample to a similar ambient but without HF. We strongly believe that this difference manifests after an initial surface roughening by HF vapor, which then speeds up condensation and droplet formation.

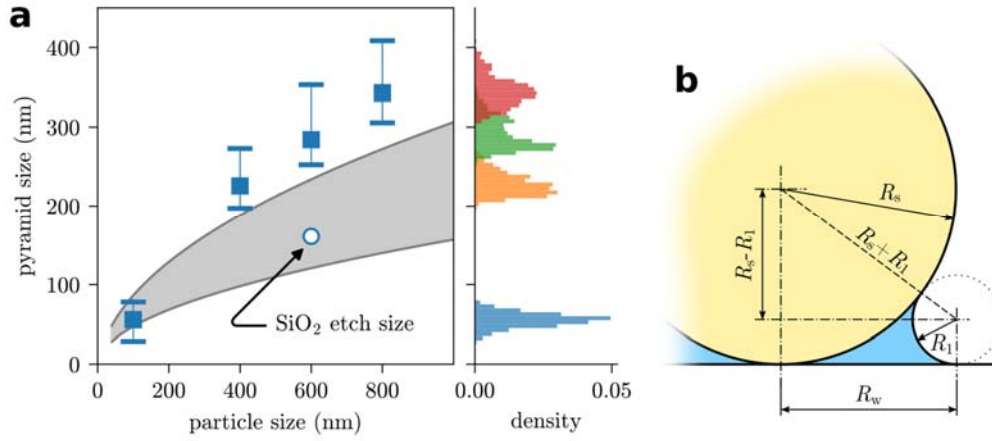


Figure 4. (a) Pyramid size distribution obtained. Squares represent the median of the distribution. As a reference, the size of the SiO₂ opening after etching for 600 nm particles is shown as a circle. The gray shaded area represents the calculated size of the meniscus for RH in the range 80% (bottom) to 95% (top). (b) Schematic of the meniscus geometry considered for calculations.

We have characterized the size of the pyramids obtained with the different colloids through SEM imaging. Pyramid sizing was automatized for the samples with 400 nm, 600 nm and 800 nm particles; however, it needed to be performed manually for the 100 nm sample. Roughly, the number of pyramids measured ranged from 400 for the manual sizing to 1000 when using the automatic image analysis. Results are shown in Figure 4, where the squares mark the mode of the size distribution, while bars indicate the full range of the data. The measured size distribution is also shown on the right for convenience. As the results clearly show, there is a direct dependence between the particle and the final pyramid sizes; the larger the particle the larger the final pyramid. More precisely, the size of the pyramids depends on the size of the HF-rich water meniscus that forms between the particle and the sample, which, in turn, depends on the size of the particle as well as the ambient relative humidity and contact angles at the SiO₂ and PS surfaces. Figure 4b shows schematically the geometry of the condensed water meniscus, where the nodoid shape of the meniscus is simplified by a circular shape with radius R_1 , as it is common practice. For the sake of simplicity, since we are in a non-equilibrium situation at the nanoscale, we will further assume that the contact angle is zero on both the substrate and the particle. The radius of the wetted SiO₂ region can, then, be calculated as

$$R_w = \sqrt{(R_s + R_1)^2 - (R_s - R_1)^2} = 2\sqrt{\frac{R_s}{k}}, \quad (1)$$

where R_s is the radius of the nanoparticle and $k=1/R_1$ is the curvature of the meniscus. The curvature of the meniscus can be related to the RH through the Laplace-Kelvin equation:

$$\gamma k = \frac{RT}{V_m} \ln\left(\frac{p}{p_0}\right), \quad (2)$$

where γ is the surface tension, R is the universal gas constant, T is the temperature, V_m is the molar volume of the liquid phase, p is the vapor pressure and p_0 is the saturation vapor pressure. Assuming that the HF concentration is low enough so that the typical water constants can be used, with the

relative humidity $RH=p/p_0$, equations 1 and 2 readily allow one to calculate the size of the etched SiO_2 region as a function of particle size and RH. In figure 4a we have included in gray the diameter of the wetted region for a RH in the range 80 % to 96 %. The experimental size of the pyramids vs. the particle size follow a similar trend to the size of the meniscus, but with larger sizes. Notice that the whole distribution of pyramid sizes is expected to be above the wetting size as it can be easily by the TMAH etching process, *i.e.* by the irregularities of the openings and the slight underetching, as well as due to the effect of the 10'' HF dip done right before the pyramid formation. In figure 4a we have also included (open circles) the size of the SiO_2 etched area measured right after the vapor etching for the 600nm sample (see fig. 3). This size, smaller than the final pyramid sizes, is perfectly consistent with the theoretical estimations and coincides, roughly, with the meniscus obtained for a RH = 90 %. Notice that, although beyond the scope of this work, figure 4a strongly suggest that the size of the pyramids can probably be controlled through a fine control of the RH during the vapor-phase treatment.

Finally, it should be mentioned that the typical pyramid size for the 100 nm case is smaller than expected. Although this deviation could just flag the limits of the simple model considered, it also could be attributed to the fact that the process only worked in a small portion of the sample surface in that particular case, while the process worked flawlessly for the rest of particle sizes. Therefore, the average pyramid size for 100 nm particles is not representative of the standard process conditions. The difficulties we experienced with the 100 nm particles could most probably be related to the lower quality monolayers that we were able to produce (see fig. 2): particles were not perfectly close packed and a double layer was mostly obtained. On the other hand, it may also indicate that the process conditions for the HF-vapor treatment need a slight fine tuning for the smallest particles size.

3 Conclusions

In this work we have introduced a method to locally deliver, with nanoscale resolution, a chemical in vapor phase through capillary condensation. In particular, the chemicals condensate in the meniscus at a nanoparticle/substrate interface. The process is simple, scalable, does not require functionalizing the nanoparticles, and it might potentially be applicable to different materials and chemicals. As a proof of concept, in this work we demonstrate the proposed process by periodically patterning a thin SiO_2 layer using a self-assembled monolayer of polystyrene particles exposed to HF vapor. The patterned SiO_2 layer is then used as a mask to create an arrangement of inverted nanopyramids on Si. The silicon nanopatterning has been demonstrated for particle sizes from 800 nm down to 100 nm using the exact same process conditions for all samples, demonstrating the robustness and repeatability of the process.

4 Acknowledgments

This work has been financially supported through the following projects: ENE2015-74009-JIN funded by the Spanish Ministry of Economy and Competitiveness (MINECO) and the European Regional Development Fund (ERDF-EU), TEC2017-82305-R (MINECO), the InnoEnergy PhD School Programme and the European Institute of Technology (EIT).

5 References

- 1 H. J.M. Veendrick, *Nanometer CMOS ICs, From basics to ASICs, 2nd edition*, Springer, 2017.
- 2 Y. Liu and X. Zhang, “Metamaterials: a new frontier of science and technology” *Chem. Soc. Rev.*, 2011, **40**, 2494–2507.
- 3 S. Jahani and Z. Jacob “All-dielectric metamaterials” *Nat. Nanotech.*, 2016, **11**, 23–36.
- 4 M. Khorasaninejad and F. Capasso “Metalenses: Versatile multifunctional photonic component” *Science*, 2017, **358**, 1146.
- 5 W. L. Barnes, A. Dereux, and T. W. Ebbesen “Surface plasmon subwavelength optics” *Nature* **424**, 824–830 (2003).
- 6 Y. Shen, C. S. Friend, Y. Jiang, D. Jakubczyk, J. Swiatkiewicz and P. N. Prasad “Nanophotonics: Interactions, Materials, and Applications” *J. Phys. Chem. B*, 2000, **104**, 7577–7587.
- 7 X. Liu, P. R. Coxon, M. Peters, B. Hoex, J. M. Cole and D. J. Fray, “Black silicon: fabrication methods, properties and solar energy applications” *Energy Environ. Sci.*, 2014, **7**, 3223.
- 8 C. Wagner, and N. Harned “EUV lithography: Lithography gets extreme” *Nat. Photonics*, 2010, **4**, 24–26.
- 9 V. R. Manfrinato, L. Zhang, D. Su, H. Duan, R. G. Hobbs, E. A. Stach and K. K. Beergg “Resolution Limits of Electron-Beam Lithography toward the Atomic Scale” *Nano Lett.*, 2013, **13**, 1555–1558.
- 10 Z. Liu, A. Shah, T. Alasaarela, N. Chekurov, H. Savin and I. Tittonen “Silicon dioxide mask by plasma enhanced atomic layer deposition in focused ion beam lithography” *Nanotechnology*, 2017, **28**, 085303.
- 11 S. Y. Chou, P. R. Krauss and P. J. Renstrom “Imprint Lithography with 25-Nanometer Resolution” *Science* **272**, 85–87 (1996).
- 12 R. D. Piner, J. Zhu, F. Xu, S. Hong and C. A. Mirkin “«Dip-Pen» Nanolithography” *Science*, 1999, **283**, 661–663.
- 13 R. Garcia, A. W. Knoll and E. Riedo “Advanced scanning probe lithography” *Nat. Nanotechnol.*, 2014, **9**, 577–587.
- 14 C. M. Bates, M. J. Maher, D. W. Janes, C. J. Ellison and C. G. Willson, “Block Copolymer Lithography” *Macromolecules*, 2014, **47**, 2–12.
- 15 S. P. Bhawalkar, J. Qian, M. C. Heiber and L. Jia “Development of a Colloidal Lithography Method for Patterning Nonplanar Surfaces” *Langmuir*, 2010, **26**, 16662–16666.
- 16 O. D. Velev and S. Gupta “Materials Fabricated by Micro- and Nanoparticle Assembly – The Challenging Path from Science to Engineering” *Adv. Mater.*, 2009, **21**, 1897–1905.
- 17 P. Colson, C. Henrist and R. Cloots “Nanosphere Lithography: A Powerful Method for the Controlled Manufacturing of Nanomaterials” *J. Nanomater.*, 2013, **2013**, 948510.
- 18 K. Chen, T. D. Dao and T. Nagao “Tunable Nanoantennas for Surface Enhanced Infrared Absorption Spectroscopy by Colloidal Lithography and Post-Fabrication Etching” *Sci. Rep.*, 2017, **7**, 44069.
- 19 C. L. Cheung, R. J. Nikolić, C. E. Reinhardt and t. F. Wang “Fabrication of nanopillars by nanosphere lithography” *Nanotechnology*, 2006, **17**, 1339–1343.

- 20 N. Chaturvedi, E. Hsiao, D. Velegol and S. H. Kim “Maskless Fabrication of Nanowells Using Chemically Reactive Colloids” *Nano Lett.*, 2011, **11**, 672–676.
- 21 J. R. Oh, J. H. Moon, S. Yoon, C. R. Park and Y. R. Do “Fabrication of wafer-scale polystyrene photonic crystal multilayers *via* the layer-by-layer scooping transfer technique” *J. Mater. Chem.*, 2011, **21**, 14167.
- 22 J. C. Brosheer, F. A. Lenfesty and K. L. Elmore “Vapor pressure of hydrofluoric acid solutions” *Ind. Eng. Chem.*, 1947, **39**, 423–427.
- 23 B. L. Weeks and J. J. DeYoreo “Dynamic meniscus growth at a scanning probe tip in contact with a gold substrate” *J. Phys. Chem. B*, 2006, **110**, 10231–10233.
- 24 C. R. Helms and B. E. Deal “Mechanics of the HF/H₂O vapor phase etching of SiO₂” *J. Vac. Sci. Technol. A*, 1991, **10**, 806–811.
- 25 B. L. Weeks and M. W. Vaughn “Direct imaging of meniscus formation in atomic force microscopy using environmental scanning electron microscopy” *Langmuir*, 2005, **21**, 8096–8098.